# MULTIPASS SAR PROCESSING FOR RADAR DEPTH SOUNDER CLUTTER SUPPRESSION, TOMOGRAPHIC PROCESSING, AND DISPLACEMENT MEASUREMENTS

Bailey Miller, Gordon Ariho, Dr. John Paden, Dr. Emily Arnold

University of Kansas Center for Remote Sensing of Ice Sheets Lawrence, KS

#### **ABSTRACT**

Differential Interferometric Synthetic Aperture Radar (DIn-SAR) processing techniques applied to ice penetrating radar enable precise measurement of the vertical displacement of englacial layers within an ice sheet. This technique has primarily been applied using ground based ice-penetrating radar due to the ability to achieve a near-zero spatial baseline. We investigate this technique on data from the Multichannel Coherent Radar Depth Sounder (MCoRDS), an airborne ice penetrating radar, and produce initial results from a high accumulation region near Camp Century in northwest Greenland. We estimate the vertical displacement by compensating for the spatial baseline using precise trajectory information and estimates of the cross-track layer slope from direction of arrival analysis. The measurement accuracy is still being investigated.

Index Terms— Multipass, InSAR, DInSAR, radar sounder

# 1. INTRODUCTION

Recent advances in ice penetrating radars and signal processing algorithms provide new and more precise measurements of the dynamic ice sheets. Improving ice sheet models requires glaciologists to understand and predict these systems as they evolve through time. In the past two decades, many ground based ApRES [1] units have been deployed to successfully measure the vertical velocity field of ice sheets using DInSAR [2]. The measurement accuracy is good, in part, because the unit can be precisely positioned so as to eliminate the spatial baseline which would otherwise lead to measurement errors due to the imprecisely known direction of arrival. For airborne data, the spatial baseline is not zero and this leads to increased displacement measurement errors.

The scattering sources for these DInSAR measurements are quasi-specular near-horizontal englacial layers throughout the ice column. See Figure 1 for an example of an internal layer and propagation rays,  $\mathbf{r}_a$  and  $\mathbf{r}_i$ , to a particular layer. Because of the near-horizontal slope, the direction of arrival

Support provided by NSF OPP-1739003.

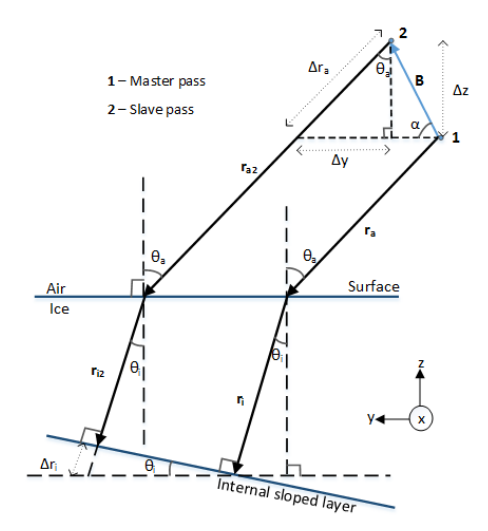


**Fig. 1**: Multipass geometry

of the layer scattering,  $\theta_i$ , comes from near nadir. The layers slowly thin or thicken over time causing the time delay to the layer to change. By measuring the phase difference between two radar passes taken at different times and using the propagation speed in ice, the average vertical velocity of the reflector can be precisely estimated.

The interferometric phase is derived in Equation (1) based on the cross-track geometry shown in Figure 1. The derivation assumes a zero along-track, x-dimension, slope and exact positioning in along-track between the two passes. Also, without loss of generality we assume the ice surface is flat since we can always transform into a coordinate system that makes the surface flat. Let B be the baseline vector between the passes,  $k_a$  be the wavenumber in air,  $k_i$  be the wavenumber in ice,  $\theta_a$  be the Direction of Arrival (DoA) of the signal in air,  $\theta_i$  be the DoA within the ice which is also equal to the cross-track slope of the internal layer. The phase change,  $\Delta \phi_a$ , between the two passes within air is given by:  $\Delta \phi_a = -k_a (\mathbf{r}_a - \mathbf{r}_{a2}) = -k_a (\Delta \mathbf{r}_a)$ , and for ice, we obtain a complementary result:  $\Delta \phi_i = -k_i (\Delta \mathbf{r}_i)$ , where  $\Delta r_a = B_z/\cos(\theta_a)$  and  $\Delta r_i = (B_z \tan(\theta_a) + B_y)\sin(\theta_i)$ . With some algebraic manipulation, the interferometric phase,

 $\phi$ , simplifies to:

$$\phi = -k_a \left[ B_z \cos(\theta_a) - B_y \sin(\theta_a) \right], \tag{1}$$

where  $B_z$ , and  $B_y$  are the z and y coefficients of **B** respectively.

A first order approximation to this function can be found using a small angle approximation for  $\theta_a$ . This leads to the following simplified form that is used to produce the results in this paper:

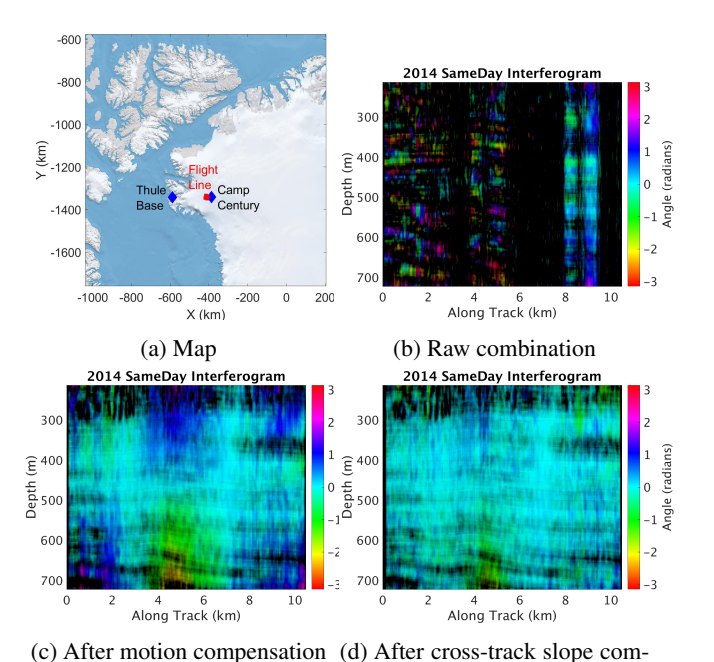
$$\phi \approx -k_a \left( B_u \sin(\theta_a) - B_z \right) \tag{2}$$

In regular side looking DInSAR, the image coregistration isolates the target in space: when coregistered pixels from two different images are compared, they correspond to the same target position. In the sounder geometry with specular layers where the propagation vector is normal to the surface, coregistration does not isolate the same target; the measured target is always the part of the surface which is normal to the range vector as shown in Figure 1. Therefore, if there is a spatial baseline, the effective scattering phase center will be shifted so that it lies at the point on the surface which is normal to the range vector. If the layer is sloped, this shift will cause a change in the two way travel time which must be compensated for to measure the vertical velocity. Since the layer slopes do change slowly with depth, this will result in a vertical velocity error which is depth dependent. Ice sheets also have a depth dependent horizontal velocity which will manifest as a depth dependent baseline error from a Lagrangian point of view.

We focus on evaluating DInSAR for airborne platforms and investigate its use on airborne data from the MCoRDS developed by the Center for the Remote Sensing of Ice Sheets (CReSIS) [3]. MCoRDS is a multichannel radar which has 15 cross-track antenna elements which are used for array processing. The advantage of airborne data is that a much wider area can be covered. In the subsequent section we describe a DInSAR processing algorithm that uses data collected from repeated passes. Following this description, we present results of combined repeated pass images with varying time intervals between images. Finally, we make some concluding remarks about the current status of the work.

## 2. METHODOLOGY

The DInSAR algorithm follows these steps: 1. coregister the Sythetic Aperture Radar (SAR) images from each channel of MCoRDS and from each pass using cross-correlation and motion compensation assuming zero slope layers, 2. direction of arrival estimation using the array of coregistered images to estimate cross-track slope phase contributions, and finally 3. apply phase corrections for motion compensation using the estimated cross-track slope and estimated GPS position errors. The motion compensation and cross-track slope compensation are the primary differences in this work compared



pensation

pensation

**Fig. 2**: a) NASA OIB flight line near Camp Century in Greenland. b)-d) Interferograms as phase compensation progresses.

to previous ground based work. Each of these steps are described in detail in the following paragraphs.

To track phase compensation progress through the algorithm, three interferograms have been generated at differing levels of compensation as the data progresses through the multipass algorithm. All available MCoRDS channels are averaged for each pass before forming the interferogram. The flight line is highlighted in red in Figure 2a. Combining with no compensation is referred to as the "raw combination". For the following images we selected two frames collected on the same day. Because of this we expect that the compensation should be able to align the images perfectly resulting in zero phase difference between the images apart for measurement error. We begin the algorithm analysis with the raw combination shown in Figure 2b. In this figure we see a small amount correlation between the phases of the two images and substantial phase wrapping where there is coherence.

The first step of compensation is coregistering the images onto a master image so that the pixels align. The first of coregistration projects each image onto the master image using the trajectory information followed by interpolation onto the master image pixel locations. After along-track resampling, a time-delay is applied in the frequency-domain to the slave data to compensate for the difference in elevation between flights. These coregistration steps mitigate the elevation and along-track offsets, but work on the assumption that the layers are perfectly horizontal and the flight paths are level. Figure 2c shows the effects of these motion compen-

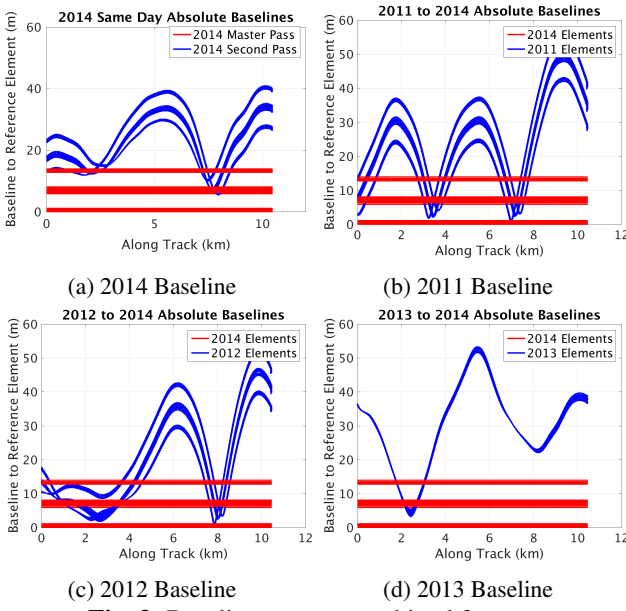


Fig. 3: Baselines across combined frames

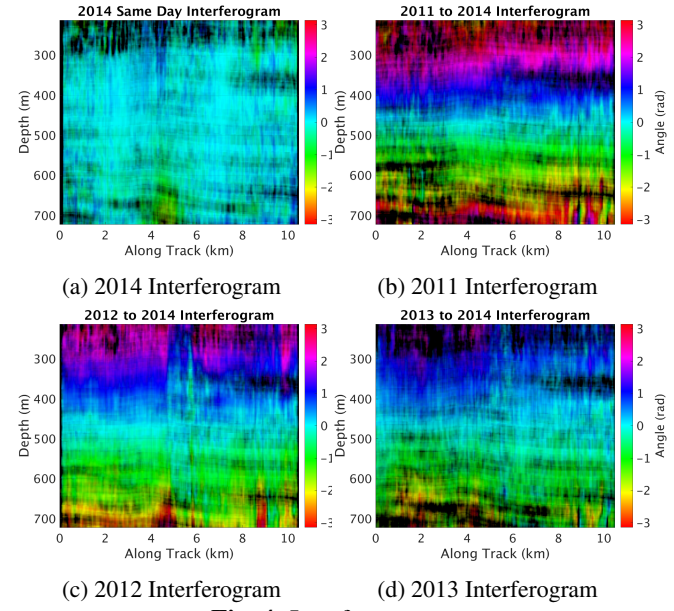


Fig. 4: Interferograms

sation steps where there is now significantly less phase wrapping and more coherence than in Figure 2b.

Once the motion compensation is complete, the images are combined using the Multiple Signal Classification (MUSIC) array processing method. Array processing combines the images together to estimate the DoA of the returned signal. DoA estimation is vital for the final step: cross-track slope compensation. The DoA is found by finding the peak in the MUSIC spectrum, culling low amplitude peaks, and spatially averaging the remaining peaks under the assumption that cross-track slope is slowly varying in depth and along-track. For the example imagery shown which uses two passes with MCoRDS for a total of 30 images (15 images per pass), we found cross-track slopes were between zero and one degree with an estimated accuracy of approximately  $\pm 0.05 \deg$  based on the width of the MUSIC peak.

The process of cross-track slope compensation follows the above steps, but applies a phase correction after motion compensation and before array processing that is based on the estimated cross-track slope. The phase correction is related to the slope by Equation (2). We next correct for GPS elevation errors between the two passes. This is compensated for by using a 2D window of pixels in the interferogram to estimate the phase at a particular depth for each range line and then shifting the phase of the whole range line by the negation of this phase. The resulting interferogram is shown in Figure 2d. There are still a few non-zero trends in the interferogram which we are investigating, but the near-zero phase result suggests that the compensation steps are successful.

### 3. RESULTS AND DISCUSSION

This section presents preliminary results using the algorithm described above. Passes are combined with a time separation of the same day, one year, two years, and three years. The master pass for all results is the example frame from the previous section which was taken in 2014. Each pass produces an image from each of the 15 antenna elements: 4 on the left wing, 7 on the fuselage, and 4 on the right wing. In 2013 only the 7 fuselage elements were installed to save costs. The plots presented in this section show the baseline between each pass and the master pass, the interferograms, and the interferogram coherence. The last plot shows estimated vertical strain rates based on the phase ramp within the interferograms.

The first plots shown in Figure 3 are the baselines to give an idea of the amount of separation between flights. The baselines vary from a maximum of 0 m to about 60 m. These plots show the absolute baseline length including horizontal and elevation offsets. (After co-registration the along-track is assumed to be zero.) The horizontal offset is generally <10 m and most of the baseline is due to elevation offsets. Elevation offsets produce a smaller effect on the interferometric phase error from cross-track slopes.

Figure 4 shows the interferometric phase for each pair of passes. The interferometric phase is computed as  $\phi = \phi_{slave} - \phi_{master}$ . All 15 (7 in 2013) images from each pass are averaged before forming the interferometric phase between the passes. As the time separation decreases, the phase wrapping reduces since the phase wrapping represents the integration of the vertical strain rate of the ice sheet over time. The longer the integration, the greater the accumulation displacement will be. Due to the ice physics at this location, the layers at the top of the image are moving away from the

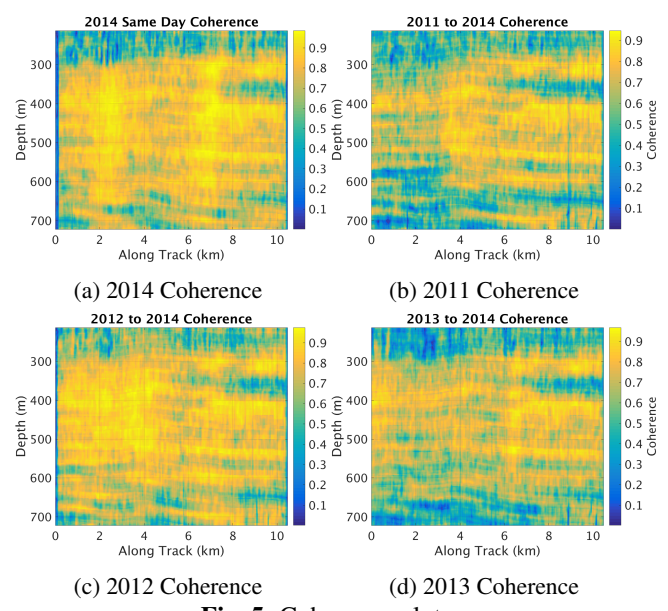


Fig. 5: Coherence plots

radar faster than the layers at the bottom. (The layer displacement reduces to zero at the base of the ice several 100 meters below where this image cuts off.) Therefore, as we travel back in time, the layers at the top of the image would have been closer and closer to the radar and this is the cause of the increasing positive phase toward the top of the image. The opposite is true toward the bottom of the images. The coherence for each interferogram is shown in Figure 5. The phase and coherence are estimated using an 9 by 45 boxcar window.

Estimating the vertical strain rate or change in velocity with depth is done by estimating the slope of the phase ramp present within the interferogram images. At this location, the vertical strain rate is expected to be greatest at the surface and decrease in rate until it approaches zero at the bedrock. These interferograms are taken in the middle of the ice and we assume the strain rate is constant with depth (although it should have a slowly decreasing trend). Figure 6 shows the strain rate calculated for the one year, two year, and three year interferograms and using the entire time gate of each interferogram to estimate the phase ramp. The phase ramp is estimated using an oversampled FFT of the interferogram. The measured phase ramp is then converted to a physical length, divided by the depth range over which the FFT was taken (to give the change in displacement as a function of depth), and finally divided by the time difference to give the strain rate. Since we expect the strain rate to be uniform with time and only slowly varying over space in this region, the 2013-2014 results appear to be lower quality on the left side of the image since they are inconsistent with the other passes.

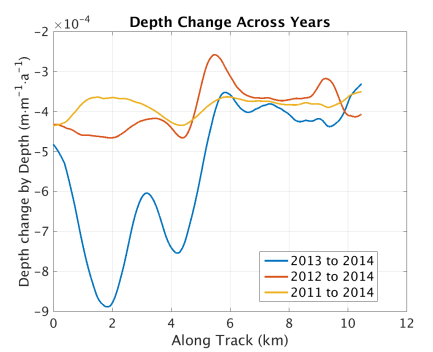


Fig. 6: Depth change depth estimates

#### 4. CONCLUSIONS

Although not all of the interferometric phase is compensated for in the same day interferogram pass, the majority is accounted for indicating that airborne DInSAR is possible with MCoRDS data. The strain rate measurements are consistent except for the 2013 pass which shows a large error for a portion of the flight line. We plan to apply the algorithm to additional flights from the decade long NASA Operation Ice-Bridge mission which flew MCoRDS on many repeat passes.

#### 5. ACKNOWLEDGEMENTS

We acknowledge the use of data from CReSIS generated with support from NASA NNX16AH54G, NSF ACI-1443054, OPP-1739003, and IIS-1838230, Lilly Endowment Incorporated, and Indiana METACyt Initiative.

## 6. REFERENCES

- [1] K. Nicholls, H. Corr, C. Stewart, L. Lok, P. Brennan, and D. Vaughan, "A ground-based radar for measuring vertical strain rates and time-varying basal melt rates in ice sheets and shelves," *Journal of Glaciology*, vol. 61, no. 230, pp. 1079–1087, 2015.
- [2] R. Bamler and P. Hartl, "Synthetic aperture radar interferometry," *Inverse Problems*, vol. 14, no. 4, pp. R1–R54, Aug 1998.
- [3] F. Rodriguez-Morales, D. Gomez-Garcia, E. Arnold, R. Hale, S. Keshmiri, C. Leuschen, J. Li, J. Paden, and C. Cardenas, "Radar systems for ice and snow measurements onboard manned and unmanned aircraft," *IEEE Latin America Transactions*, vol. 16, no. 9, pp. 2473– 2480, 2018.